J. Wurts, J. L. Stein, and T. Ersal, "Minimum Slip Collision Imminent Steering in Curved Roads Using Nonlinear Model Predictive Control," American Control Conference, Philadelphia, PA, USA, pp. 3975-3980, 2019.

Minimum Slip Collision Imminent Steering in Curved Roads Using Nonlinear Model Predictive Control

John Wurts, Jeffrey L. Stein, and Tulga Ersal*

Abstract— **Previous work by the authors has introduced a collision imminent steering algorithm to autonomously steer a vehicle if an imminent collision cannot be avoided by braking alone. The original formulation was developed for straight roads. In this work, a new formulation is presented to account for curved roads, as well. To accommodate curved roads, a drivable tube is introduced, within which any trajectory is considered collision free. The optimal control problem is formulated to minimize the peak tire slip of the maneuver to seek a minimally aggressive solution. To ensure the safety of the vehicle in a potential maneuver, hard safety constraints on the vehicle stability and safe driving regions are enforced. Numerical simulations are presented to demonstrate the effectiveness of the proposed formulation.**

I. Introduction

Automotive active safety features are designed to automatically augment or even override drivers in the event of unsafe driving situations. As next generation automobiles incorporate advanced hardware and improved computing platforms, new active safety features can be incorporated. Collision imminent steering (CIS) is one such feature that is designed to actively perform a lane change in the event a forward collision cannot be avoided by breaking alone. As such, this is a safety critical maneuver that may push the vehicle to its dynamic limits of handling, but must not exceed them. Therefore, the primary control challenge with enacting a CIS maneuver is to determine the optimal control trajectory, and corresponding state trajectory. These trajectories are situation dependent and therefore not known *a priori*.

To address this challenge, previous research has developed a one-level nonlinear model predictive control (MPC) formulation for straight roads to ensure the state trajectory is feasible by the nonlinear vehicle dynamics and obeys hard safety considerations through numerical optimization constraints [1]. This paper extends this formulation to handle more general environments such as curved roads, as well.

CIS, as well as the larger problem of obstacle avoidance, has been studied at various levels of environmental complexity. To incorporate hard safety constraints, two-level linear [2] and two-level nonlinear [3] MPC controllers have enforced lateral displacement limits as numerical constraints in the optimization formulation. In these works, the MPC controller aims to track a reference trajectory by a PID fitness metric, but also monitors the lateral displacement in the prediction trajectory. If the lateral displacement from the reference trajectory is exceeded, the controller adjusts the trajectory to maintain displacement bounds, and then incorporates the objective function as a secondary factor. Although the controller is able to maintain hard safety constraints while regulating deviation from the reference trajectory, there are two key drawbacks. First, the controller is reliant on a reference trajectory to begin with, which, in general, is not known *a priori*. Second, the lateral displacement bounds must be explicitly defined at each time step to build the optimization problem, and thus relies on an additional layer to map the drivable space to deviation limits.

To address the first limitation, one-level MPC architectures have been developed, which handle the optimal path planning and path tracking simultaneously. Specific to a lane change maneuver, one-level linear MPC has been applied to a double lane change to study blended control [4]. In said work, two adjacent lanes are modeled and the vehicle is allowed to change lanes as it sees fit. Hard safety constraints are implemented by designing lateral displacement bounds to force a lane change prior to encountering an obstacle in the current lane, and then to return to the original lane after clearing the obstacle. While the controller is able to avoid collision, the formulation is based on linearized dynamics and the lane change procedure is described by an explicit bound on the y lateral displacement, which can only model straight road implementations [1].

In the context of the second limitation, the reviewed methods are not able to directly map environmental information into the optimization problem. Instead, the environmental information is mapped from its native x-y state space representation to time discrete space correlating with the predicted state trajectory. This multistage process can be challenging for three reasons. First, the time discrete environmental representation can change from one time step to the next in closed-loop control [3]. This discrete change can cause issues for gradient-based optimization, creating a more computationally expensive problem. Second, as the trajectory morphs during the MPC optimization, the environmental information relevant to each time step can change discretely, leading to the same gradient issues. Third, the additional mapping of state information and obstacle information to discrete time space to compute allowable lateral displacement bounds creates computational overhead compared to directly handling obstacle information in pure x-y state space.

In comparison to the state of the art reviewed above, the salient contribution of the CIS controller presented in this

* Corresponding author (tersal@umich.edu)

J. Wurts, J.L. Stein, and T. Ersal are with the Department of Mechanical Engineering, University of Michigan, Ann Arbor, MI.

Toyota Research Institute ("TRI") provided funds to assist the authors with their research, but this article solely reflects the opinions and conclusions of the authors and not TRI or any other Toyota entity.

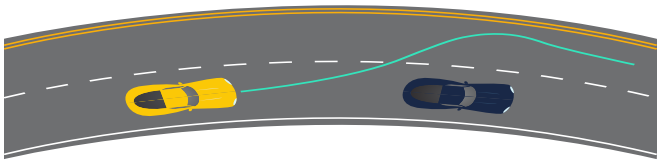

Fig. 1. The host vehicle, yellow, encounters the obstacle, blue. A candidate trajectory is drawn in teal, where the host has completely changed lanes when crossing the obstacle, remains within the road boundary throughout, and is centered in the new lane at the end of the maneuver.

paper is incorporating abstract driving environment information, as described by a drivable tube, directly into the feasibility definition of the CIS maneuver. By incorporating environmental information through x-y state space, the MPC optimization problem does not require lateral displacement bounds to be explicitly defined at each time step, nor does it rely on a reference trajectory to begin with. This allows the CIS formulation to be extended to include curved roads, increasing the environmental complexity the CIS controller can operate in.

The remainder of the paper is structured as follows. First, details on the curved highway environment and drivable space, as well as host vehicle and corresponding vehicle dynamics are contained in Sec. II. Second, optimal control formulation including objective function and safety constraints are derived in Sec. III. Numerical simulation results and their interpretations are reported in Sec. IV. Finally, conclusions and future directions are given in Sec. V.

II. Drivable Space and Vehicle Dynamics Model

A highway driving environment is the most likely scenario of a CIS maneuver due to the high driving speed. For the proposed scenario, hard safety constraints are enforced by ensuring the vehicle remains within the lane boundaries, which is captured by the drivable tube [5].

The drivable tube can be generated from online evaluation of the current environment through the use of cameras, LIDAR, high definition GPS maps, and other sensor information. For the purposes of the numerical analysis in Sec. IV, a drivable tube is generated geometrically from a simulated highway environment. The following derivation of the geometric drivable tube is included only to generate an input to the CIS controller; actual implementation would require online generation.

Fig. 1 shows an outside lane change as a candidate CIS maneuver. The host vehicle starts centered in the right lane and identifies a stationary obstacle. A candidate trajectory is overlaid, which shows the host vehicle changing lanes before crossing the obstacle, remaining inside the outer lane boundary, and then stable at the end of the maneuver.

To explore a highly challenging scenario, the highway curvature is chosen to push the vehicle to its upper limits of performance. A target highway speed of $u_0 = 35$ m/s (78 mph) is chosen, as it is on the faster side of acceptable highway speeds in the United States. For the chosen target speed, US highway building regulations dictate the minimum turn radius as about $1{,}500$ m [6], but, to test a more aggressive maneuver and make the impact of curvature more prominent, a turn radius of $r_{\text{turn}} = 500$ m is chosen.

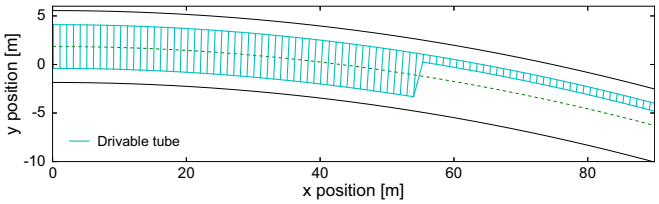

Fig. 2. The drivable tube for the lane change in teal, as well as the approximate lane markings. The drivable tube shrinks as it passes the obstacle, and is contracted narrower than the lane width to account for the vehicle half width.

Additionally, the minimum highway lane width is defined as $w_{\text{lane}} = 3.7$ m [7]. An obstacle is set stationary at a distance $d_{\text{obstacle}} = 55$ m along the arc of the center of the middle lane. The distance of 55 m is chosen, as it is inside the safe braking distance, but is still far enough to perform a lane change safely [1]. In practice, obstacle information would be available from online sensors and incorporated into the drivable tube.

The hard safety constraint of keeping the vehicle inside the drivable space relies on a sequence of connected quadrangles, and is derived later in Sec. III. The drivable space is the topographical area of the lanes the vehicle can safely occupy, and a set of successive quadrangles within the drivable space forms the drivable tube.

For this maneuver, the drivable space is both left and right lanes until reaching the obstacle, then only the left lane thereafter. However, the prediction vehicle model, a 3 degrees of freedom (DoF) bicycle model described later in this section, only considers the vehicle's center of gravity (CG). As such, modifications to the drivable space must be made to account for the width of the vehicle. For a given vehicle width, w_v, and safety margin to account for vehicle rotation, $\sigma = 0.5$ m, the drivable boundaries are squeezed to the center of the lane. This implies that before crossing d_{obstacle}, the right boundary follows a curvature of $r_{\text{turn}} - \frac{w_{\text{lane}}}{2} + w_v + \sigma$, and the left boundary follows a curvature of $r_{\text{turn}} + \frac{3w_{\text{lane}}}{2} - w_v - \sigma$. After passing the obstacle, the drivable space is completely restricted to the left lane, thus the right edge boundary is $r_{\text{turn}} + \frac{w_{\text{lane}}}{2} + w_v + \sigma$, and the left boundary remains the same.

Consider a global coordinate frame with the vehicle centered at the origin. The lanes are described by arcs centered at $(x_c, y_c) = (0, -r_{\text{turn}})$. The right and left edges of the drivable tube are calculated by taking discrete arc steps and storing the x and y position of the edge in a right and left boundary array. The four points corresponding to the two pairs at a given array index k and next step $k+1$ form one quadrangle.

Using this methodology, Fig. 2 shows the drivable tube for the right and left lane changes. Note, to avoid a quadrangle of zero length, a transition quadrangle is used immediately before the obstacle.

Consider next the details of the prediction model dynamics. The prediction model mirrors previous work [1], which provides an in depth derivation. The prediction model is a 3DoF bicycle model with active four wheel steering and Pacejka magic tire forces. The use of a simplified 3DoF bicycle model is based on previous studies that have shown this is

TABLE I

HOST VEHICLE PARAMETERS BASED ON 2018 BMW 740*i*

Vehicle Parameter	Parameter Symbol	Value
Vehicle mass	m	1982 kg
Weight distribution	-	51.4/48.6 F/R
Wheel base	-	3.2 m
Vehicle width	w_v	1.9 m
Front wheel to CG distance	l_f	1.56 m
Rear wheel to CG distance	l_r	-1.64 m
Front wheel vertical force	$F_{z,f}$	1016
Rear wheel vertical force	$F_{z,r}$	966
Yaw moment of inertia	I_{zz}	4892 kg$\cdot$m^2

The upper table is values from manufacturer's technical specification. The lower table is values derived as needed for 3DoF model.

sufficiently accurate for MPC-based obstacle avoidance when obstacles are not excessively wide [8]. Four wheel steering controllers extend to front-only steering system by locking the rear wheels.

The host vehicle is modeled after a luxury sedan, as this class of vehicles is the most common to introduce advanced hardware and software features. Parameters relevant to the 3DoF model are given in Table I, and Pacejka tire parameters in Table II.

The vehicle states, control inputs, corresponding system dynamics, and nonlinear tire forces are given in (1)-(4).

$$\mathbf{x} = \begin{bmatrix} \text{global x position [m]} \\ \text{global y position [m]} \\ \text{vehicle yaw [rad]} \\ \text{longitudinal velocity [m/s]} \\ \text{lateral velocity [m/s]} \\ \text{yaw rate [rad/s]} \\ \text{front steering angle [rad]} \\ \text{rear steering angle [rad]} \end{bmatrix} = \begin{bmatrix} x \\ y \\ \psi \\ u \\ v \\ \omega \\ \delta_f \\ \delta_r \end{bmatrix} \tag{1}$$

$$\mathbf{u} = \begin{bmatrix} \text{front steering rate [rad/s]} \\ \text{rear steering rate [rad/s]} \end{bmatrix} = \begin{bmatrix} \dot{\delta}_f \\ \dot{\delta}_r \end{bmatrix} \tag{2}$$

$$\frac{d\mathbf{x}}{dt} = \begin{bmatrix} u\ \cos(\psi) - v\ \sin(\psi) \\ u\ \sin(\psi) + v\ \cos(\psi) \\ \omega \\ 0 \\ -u\ \omega + \frac{F_{y,f}\cos(\delta_f) + F_{y,r}\cos(\delta_r)}{m} \\ \frac{F_{y,f}\cos(\delta_f) l_f - F_{y,r}\cos(\delta_r) l_r}{I_{zz}} \\ \dot{\delta}_f \\ \dot{\delta}_r \end{bmatrix} \tag{3}$$

$$\begin{aligned} F_{y,\text{-}} &= \mu F_{z,\text{-}} \sigma_{y,\text{-}} \\ \sigma_{y,\text{-}} &= -\sin\left(C\ \arctan\left(B\frac{V_{y,\text{-}}}{V_{x,\text{-}}}\right)\right) \\ V_{x,\text{-}} &= u\ \cos(\delta_\text{-}) + (v + \omega l_\text{-})\sin(\delta_\text{-}) \\ V_{y,\text{-}} &= -u\ \sin(\delta_\text{-}) + (v + \omega l_\text{-})\cos(\delta_\text{-}) \end{aligned} \tag{4}$$

In (3), $\dot{u} = 0$, implying the longitudinal velocity is locked. Fixing the longitudinal velocity is consistent with collision avoidance maneuvers, as explicit accelerations and braking are not permitted by the testing standard [9]. Later numerical results show the longitudinal acceleration due to the tire forces to be small, thus no significant loss of accuracy is incurred with fixing the longitudinal velocity.

(1)-(4) fully dictate the prediction model used in the MPC formulation. In the next section, the MPC controller is formulated and underlying numerical optimization problem developed.

III. OPTIMAL CONTROL PROBLEM AND MODEL PREDICTIVE CONTROL FORMULATION

The MPC controller uses an explicit fourth order Runge-Kutta (RK4) integration scheme to map the control trajectory to the predicted state trajectory. RK4 integration only provides the system states at each discrete time step, thus the minimum aggressive CIS maneuver criteria are developed to handle the sequence of integration states. At each time interval, the control input consists of a constant front and rear steering rate lasting $t_s = 100$ ms. The prediction horizon extends to $t_h = 3$ s, implying the control trajectory is 30 constant control inputs. The RK4 integration uses time steps of $\Delta t = 10$ ms.

The system dynamics are propagated forward over the control trajectory, resulting in a state trajectory containing the full system state at each time step. This mapping through the RK4 integration inherently enforces the system dynamics constraints typically required in MPC; thus the system dynamics constraints do not need to be explicitly defined in the numerical optimization problem. However, RK4 integration still relies on an initial starting state to propagate the dynamics forward from, which is derived in the following subsection.

A. Initial State

The host vehicle is assumed to be traveling along a stable trajectory in the initial lane when the CIS maneuver is initiated. The initial states are found by evaluating (3) for $\frac{dv}{dt} = \frac{d\omega}{dt} = 0$ for a given r_lane, u, and desired δ_f and δ_r pair. In this example, the initial stable states are used as inputs to the controller, as the methodology can incorporate instantaneous states from sensor information at implementation.

The details of establishing the initial yaw rate, ω_0, initial lateral velocity, v_0, rear steering angle, δ_r, and corresponding front steering angle, δ_f, are omitted for brevity. The initial x, y, and ψ are all set to 0 as the controller is structured in a vehicle fixed coordinate frame. The nominal states form the following initial state vector, from which the RK4 integration propagates.

$$\mathbf{x}_0 = \begin{bmatrix} 0 & 0 & 0 & u_0 & v_0 & \omega_0 & \delta_{f,0} & \delta_{r,0} \end{bmatrix}^T \tag{5}$$

B. Drivable space constraint

The drivable space, and corresponding drivable tube, forms a left and right nonintersecting boundary for the vehicle CG.

TABLE II

TIRE PROPERTIES

Tire Parameter	Parameter Symbol	Value
Coefficient of Friction	μ	0.8
Tire Property	B	13
Tire Property	C	1.285
Tire Longitudinal Velocity	V_x	
Tire Lateral Velocity	V_y	

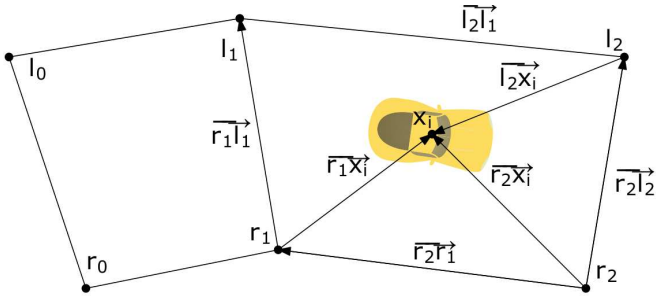

Fig. 3. The relevant vectors used in establishing the active quadrangle, and evaluating right and left edge boundary constraints.

A candidate state trajectory is considered valid if all discrete integration points are within the boundaries.

To evaluate if an integration state is within the lane boundaries, vector algebra is used both to determine the active quadrangle and to generate a constraint value. Consider Fig. 3, showing a standalone integration state and the relevant vectors. The first step is to identify the active quadrangle. Using matching indices of the left and right edge boundary, a vector is formed representing the transition from one quadrangle to the next. Consider the forward edge of the first quadrangle, denoted by $\overrightarrow{\mathbf{r}_1\mathbf{l}_1}$, representing the vector from $\mathbf{r}_1$ to $\mathbf{l}_1$. Consider next the vector representing the position of the integration point, $\mathbf{x}_i$, relative to the forward corner of the right quadrangle, $\mathbf{r}_1$, denoted $\overrightarrow{\mathbf{r}_1\mathbf{x}_i}$. The sign of the cross product $\overrightarrow{\mathbf{r}_1\mathbf{l}_1} \times \overrightarrow{\mathbf{r}_1\mathbf{x}_i}$ is used to indicate if the explicit integration state is in front of or behind the quadrangle. For the first quadrangle, this cross product is less than zero, indicating the integration point has progressed beyond that quadrangle.

Conversely, the cross product for the second quadrangle, $\overrightarrow{\mathbf{r}_2\mathbf{l}_2} \times \overrightarrow{\mathbf{r}_2\mathbf{x}_i}$, is greater than zero. The active quadrangle is established when this cross product crosses zero.

The requirement that the integration point must lie inside the edge boundaries is enforced through two individual constraints. Consider first the right edge constraint. A vector representing the right edge boundary, $\overrightarrow{\mathbf{r}_2\mathbf{r}_1}$, is crossed with the position vector, resulting in $\overrightarrow{\mathbf{r}_2\mathbf{r}_1} \times \overrightarrow{\mathbf{r}_2\mathbf{x}_i}$. If the integration state is to the left of the right lane boundary, then the cross product will be negative. Thus, the right lane edge boundary constraint is considered to be valid if $\overrightarrow{\mathbf{r}_2\mathbf{r}_1} \times \overrightarrow{\mathbf{r}_2\mathbf{x}_i} \leq 0$.

Similarly for the left edge, $\overrightarrow{\mathbf{l}_2\mathbf{l}_1}$ is crossed with the vehicle position relative to the forward left corner, $\overrightarrow{\mathbf{l}_2\mathbf{x}_i}$, to form the constraint $\overrightarrow{\mathbf{l}_2\mathbf{x}_i} \times \overrightarrow{\mathbf{l}_2\mathbf{l}_1} \leq 0$. Note, the cross product order has been switched to maintain "≤ 0" as a valid constraint.

In general, each integration state, $\mathbf{x}_i$, is contained within the fore and aft bounds of an active quadrangle k, where $\mathbf{r}_k$, $\mathbf{r}_{k+1}$, $\mathbf{l}_{k+1}$, and $\mathbf{l}_k$ form the four corners of the quadrangle. The right and left constraints are formed as follows.

$$d_r = \overrightarrow{\mathbf{r}_k\mathbf{r}_{k-1}} \times \overrightarrow{\mathbf{r}_k\mathbf{x}_i} \leq 0 \tag{6}$$

$$d_l = \overrightarrow{\mathbf{l}_k\mathbf{x}_i} \times \overrightarrow{\mathbf{l}_k\mathbf{l}_{k-1}} \leq 0 \tag{7}$$

Based on the formulation of (6) and (7), the left and right boundary must not be intersecting as well as branch-free, as both scenarios would result in unsolvable constraints.

By evaluating the lane boundary criteria through this vector algebra formulation, the discrete event of leaving the lane boundary can be captured in a continuous formulation. This avoids a mixed integer optimization problem, allowing the underlying MPC optimization to be solved using gradient-based optimization. Details on calculating sensitivities for RK4 integration and related MPC problems can be found in [1].

The right and left edge constraints are enforced at every integration point in the prediction horizon. This can create a substantial number of constraints, all of which are loosely related to each other. To reduce the size of the numerical optimization problem, these multiple constraints are aggregated into two constraints through the KS function as follows [10].

$$\mathrm{KS}(\mathbf{g}, \rho_{\text{edge}}) = \frac{1}{\rho_{\text{edge}}} \ln\Big(\sum_{i=1}^{n} e^{\rho_{\text{edge}} g_i} \Big) \tag{8}$$

Here, $\mathbf{g}$ represents the vector of left or right edge boundary constraints throughout the prediction horizon, and ρ_{edge} presents the aggregation parameter. Numerical simulation has shown $\rho_{\text{edge}} = 80$ to be numerically stable.

Recall that one limitation of the state-of-the-art methods discussed in Sec. I is the lateral deviation bounds have to be explicitly defined at each time step. Using the proposed active quadrangle approach, the trajectory bounds are a function of the x-y position, not necessarily the current time index. As the predicted state trajectory morphs during the optimization, the active quadrangle at a given time step may change, which is natively handled in the proposed methodology.

The final criterion for a successful CIS maneuver is dictating that the state trajectory is stable at the terminal state as well as stable throughout the prediction horizon. These constraints are derived in the next couple of subsections.

C. Terminal Position

One concern with a CIS maneuver is initiating a maneuver that is unrecoverable mid-maneuver. To avoid this, terminal state constraints are imposed to ensure a feasible solution sees the maneuver all the way through, and hence avoiding initiating a maneuver that may not be recoverable mid-trajectory.

The terminal state follows the same analysis presented in Sec III-A, but with a couple of adjustments. For reference, $\mathbf{x}_t$ represents the final integration state in the prediction horizon. Consider first the modified lane curvature.

The proposed CIS maneuver is a single lane change to avoid the collision and does not return to the original lane. A double lane change is possible, but would require a longer prediction horizon and thus a larger optimization problem.

For a single lane change to the outside, the terminal position is at a new lane curvature. For the new curvature, establishing stable terminal states mirrors Sec. III-A. Similar to the initial states, the terminal states are generated from a pre-established road curvature. For implementation, road curvature can be estimated online, or the terminal state constraints can be established as needed.

$$\mathbf{x}_{\text{stable}} = \begin{bmatrix} x & y & \psi & u_0 & v_t & \omega_t & \delta_{f,t} & \delta_{r,t} \end{bmatrix}^T \tag{9}$$

Note that x, y, or ψ in the terminal state do not have a subscript t, as these values are not directly enforced. This is because the numerical optimization problem does not know the terminal arc location of the state trajectory prior to simulating the control trajectory. Alternatively, the terminal x-y position is directly related to the terminal road curvature as follows.

$$(x_t - x_c)^2 + (y_t - y_c)^2 = r_t^2 \tag{10}$$

Similarly, the terminal heading is near tangential to the lane, corrected for the side slip.

$$\arctan\left(\frac{y_t - y_c}{x_t - x_c}\right) = \frac{\pi}{2} - \arctan\left(\frac{v_t}{u_0}\right) \tag{11}$$

Altogether, (9)-(11) form the stable terminal state. The second stability criterion, the vehicle remains stable throughout the maneuver, is defined through a tire slip constraint as follows.

D. Tire slip constraint

The nonlinear tire forces used in the MPC prediction model captures the force relaxation at high slip angles. Entering this relaxation region should be avoided, as the controller can quickly lose control authority [11].

To ensure tire stability, the peak tire slip angle is constrained within the stable region. Previous analysis has shown this stable tire region to be within $\alpha_{\text{peak}} \leq 8^\circ$ for this tire parameter set [1]. This forms both a front tire slip constraint and a rear tire slip constraint enforced at every integration point.

$$\alpha_{\text{-}} = \delta_{\text{-}} - \arctan\left(\frac{v + \omega\ l_{\text{-}}}{u}\right)$$
$$|\alpha_{\text{-}}| \leq \alpha_{\text{peak}} \tag{12}$$

Using the a KS function similar to Sec. III-B, both the front and rear slip constraints are aggregated as follows.

$$\text{KS}(\alpha_{\text{-}}, \rho_{\text{peak}}) = \frac{1}{\rho_{\text{peak}}} \ln\Big(\sum_{i=1}^{n} e^{\rho_{\text{peak}} |\alpha_{\text{-},i}|}\Big) \tag{13}$$

E. Objective function

The fitness of a candidate CIS maneuver is maximum tire slip. By minimizing the maximum tire slip in the maneuver, the additional control authority the vehicle needs to make mid-maneuver corrections is maximized [10].

Using *max* and *min* functions in gradient based optimization should be avoided, as it introduces discrete changes, which is not well captured by the gradient. Instead, the KS function can smoothly capture the maximum value while maintaining differentiability.

To capture this, a new vector, α^*, is formed, composed of the front and rear wheel slip angles at each integration point. The objective function is then formed as follows, with $\rho_{\text{obj}} = 80$ having been numerically robust in simulation.

$$\text{KS}(\alpha^*, \rho_{\text{obj}}) = \frac{1}{\rho_{\text{obj}}} \ln\Big(\sum_{i=1}^{2n} e^{\rho_{\text{obj}} |\alpha_i^*|}\Big) \tag{14}$$

Next, the physical constraints on the vehicle are modeled.

F. Steering angle and steering rate constraint

The host vehicle has physical limitations on the allowable steering angle and steering rate. The front wheels are allowed a peak steering angle of $\delta_{f,\max} = 35^\circ$, and a steering rate of $\dot{\delta}_{f,\max} = 70$ deg/s. The rear wheels do not have as much mobility, as they have a peak angle of $\delta_{r,\max} = 10^\circ$, and steering rate of $\dot{\delta}_{r,\max} = 35$ deg/s. Conventional front-only steering is modeled by setting $\delta_r = 0^\circ$.

At this point, all of the constraints necessary to model the desired CIS maneuver and vehicle are established. These are then combined to form the numerical optimization problem.

G. Numerical optimization problem

The corresponding numerical optimization problem is formulated as follows.

$$\begin{aligned}
\min_{\mathbf{u}} \quad & \text{KS}(\alpha^*, \rho_{\text{obj}}) & \\
\text{subject to} \quad & \text{KS}(\mathbf{d}_r, \rho_{\text{edge}}) & \leq 0 \\
& \text{KS}(\mathbf{d}_l, \rho_{\text{edge}}) & \leq 0 \\
& \text{KS}(\alpha_f, \rho_{\text{peak}}) & \leq \alpha_{\text{peak}} \\
& \text{KS}(\alpha_r, \rho_{\text{peak}}) & \leq \alpha_{\text{peak}} \\
& (\mathbf{x}_t)_i - (\mathbf{x}_{\text{stable}})_i & = 0\ \forall\ i \in [4,8] \\
& (x_t - x_c)^2 + (y_t - y_c)^2 & = r_{\text{lane}}^2 \\
& \arctan\left(\frac{y_t - y_c}{x_t - x_c}\right) & = \frac{\pi}{2} - \arctan\left(\frac{v_t}{u_0}\right) \\
& |\delta_{\text{-}}(t_i)| & \leq \delta_{\text{-},\max}\ \forall\ t_i \\
& |\dot{\delta}_{\text{-}}(t_i)| & \leq \dot{\delta}_{\text{-},\max}\ \forall\ t_i
\end{aligned} \tag{15}$$

Here, the system dynamic constraints are not explicitly introduced into the optimization problem, because these are directly incorporated by the RK4 integration. Any trajectory that satisfies the constraints of (15) is considered to be a valid CIS maneuver, and of the set of valid CIS maneuvers, the one with the smallest peak slip is considered to be the optimum.

In the next section, (15) is solved, and the resulting solutions are analyzed.

IV. Numerical Simulation

(15) can be solved with a variety of numerical solvers. For the solutions analyzed here, results were generated with IPOPT [12]. Solutions were found within 200 ms using a high performance desktop computer using a multiple shooting implementation with custom CUDA acceleration.

Fig. 4 shows the x-y trajectory of the CIS maneuver, as well as various vehicle states.

The outside lane change is a rather gradual maneuver. The vehicle begins the lane change by shortly steering to the left, setting up the vehicle for a second turn. Then, the vehicle makes a long, constant turn to the right, both avoiding the obstacle and obeying the outer lane boundary. At the end of the maneuver, the vehicle makes a small correction to reach the terminal states exactly, thus obeying all the constraints.

The largest tire slip experienced for this CIS scenario is approximately 3°. During the outside lane change, the

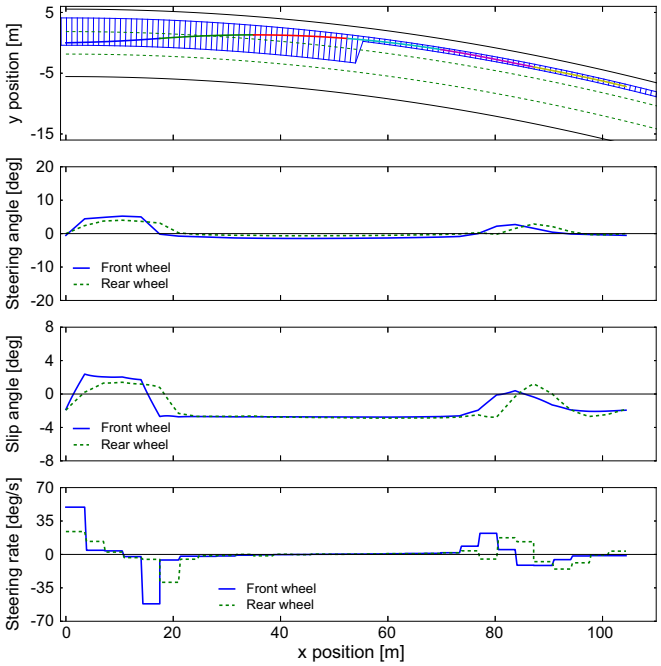

Fig. 4. CIS maneuver to the outside lane. The vehicle begins with a quick turn to the left, then continues with a long turn to the right.

vehicle reaches 3° twice. The first instance is when the vehicle initially turns to the left, reaching positive 3°. Then, when making the constant turn to the right, the vehicle maintains -3° until the corrections at the end. Overall, the outside lane change is rather gradual, as it is a short turn to the left followed by a long turn to the right.

Compared to a straight road example, the outside lane change is a less aggressive maneuver and does not reach as high of a peak tire slip. However, for the outside lane change, it is possible that the obstacle occludes the lane information further down the road. Modifications to the geometrically defined drivable tube can simulate an inside lane change as well, which is comparably more aggressive than straight road, but avoids occlusion.

Similar to previous results [10], the minimum slip formulation produces trajectories that cut as close as allowable to the lane boundaries. The resulting trajectory uses all of the allowable space, cutting close on the lane change pass and just avoiding leaving the outer lane boundary. This is consistent with the optimization formulation, as the fitness of a candidate trajectory is not how close it comes to the boundary, only that it does not leave the boundary.

V. Conclusion

In this work, a CIS controller using nonlinear one-level MPC is developed to operate in curved roads. Using geometric analysis, an artificial curved highway is developed for simulation purposes, though the presented controller can obtain highway information from other sources online. Hard safety constraints of the vehicle are enforced through constrained optimization, where feasible solutions are guaranteed to satisfy said constraints. Vehicle x-y trajectory constraints are enforced by restricting the state trajectory to within a drivable tube. Stability constraints are enforced throughout the maneuver and at the terminal position to ensure the vehicle maintains controllability throughout. Simulation results present an outside lane change, which shows the formulation can adapt to more complex environments.

One potential limitation to this formulation is that by design the vehicle is allowed to come as close as possible to the lane boundary. When real world effects such as system uncertainty and sensor noise are introduced, the vehicle might violate these constraints. Further, the controller has perfect information of the plant model, thus no plant-prediction model mismatch effects are considered. The current formulation is intended to be robust to these effects by maximizing the available tire force to make mid-maneuver corrections in closed-loop implementation, but formal robustness certification needs to be considered.

One important direction for future research is incorporating uncertainty into the controller, both in the plant-prediction model mismatch and sensor information. In the context of plant-prediction model mismatch, the controller may incorporate potential uncertainty into the prediction model; and in the context of sensor information, the controller may incorporate environmental uncertainty. Together, these considerations are expected to make the controller more robust to real world effects.

References

[1] J. Wurts, J. L. Stein, and T. Ersal, "Collision imminent steering using nonlinear model predictive control," in *2018 Annual American Control Conference (ACC)*. IEEE, 2018, pp. 4772–4777.

[2] S. Di Cairano, U. Kalabić, and K. Berntorp, "Vehicle tracking control on piecewise-clothoidal trajectories by mpc with guaranteed error bounds," in *IEEE Conference on Decision and Control (CDC)*. IEEE, 2016, pp. 709–714.

[3] M. Brown, J. Funke, S. Erlien, and J. C. Gerdes, "Safe driving envelopes for path tracking in autonomous vehicles," *Control Engineering Practice*, vol. 61, pp. 307–316, 2017.

[4] S. J. Anderson, S. C. Peters, T. E. Pilutti, and K. Iagnemma, "An optimal-control-based framework for trajectory planning, threat assessment, and semi-autonomous control of passenger vehicles in hazard avoidance scenarios," *International Journal of Vehicle Autonomous Systems*, vol. 8, no. 2-4, pp. 190–216, 2010.

[5] S. M. Erlien, S. Fujita, and J. C. Gerdes, "Safe driving envelopes for shared control of ground vehicles," *IFAC Proceedings Volumes*, vol. 46, no. 21, pp. 831–836, 2013.

[6] A. A. O. S. Highway and T. Off, *A Policy on Geometric Design of Highways and Streets 2001*. American Association of State Highway Transport., 2001.

[7] U. D. of Transportion, *Speed Concepts: Informational Guide*. Federal Highway Administration, 2009.

[8] J. Liu, P. Jayakumar, J. L. Stein, and T. Ersal, "A study on model fidelity for model predictive control-based obstacle avoidance in high-speed autonomous ground vehicles," *Vehicle System Dynamics*, vol. 54, no. 11, pp. 1629–1650, 2016.

[9] Y. Peng and X. Yang, "Comparison of various double-lane change manoeuvre specifications," *Vehicle System Dynamics*, vol. 50, no. 7, pp. 1157–1171, 2012.

[10] J. Wurts, J. L. Stein, and T. Ersal, "Collision imminent steering at high speed using nonlinear model predictive control," *Transactions on Vehicle Technology, under review*, 2018.

[11] J. Liu, P. Jayakumar, J. L. Stein, and T. Ersal, "A nonlinear model predictive control formulation for obstacle avoidance in high-speed autonomous ground vehicles in unstructured environments," *Vehicle System Dynamics*, pp. 1–30, 2017.

[12] A. Wächter and L. T. Biegler, "On the implementation of an interior-point filter line-search algorithm for large-scale nonlinear programming," *Mathematical Programming*, vol. 106, no. 1, pp. 25–57, 2006.